buildings

MDPI

Article

Three-Dimensional Printable Concrete by an Ultra-Thin Nozzle and Fully Sealed Extrusion

Jing Shen [1], Yujia Li [2], Xiaoman Zhang [1], Yangbo Li [2], Chaohui Huang [3] and Wei Luo [3,*]

[1] School of Transportation Science and Engineering, Beihang University, Beijing 100191, China; chenjing0813@buaa.edu.cn (J.S.); zy2213209@buaa.edu.cn (X.Z.)
[2] College of Hydraulic and Environmental Engineering, China Three Gorges University, Yichang 443002, China; lyj121341046@163.com (Y.L.); liyangbo@ctgu.edu.cn (Y.L.)
[3] Haining Yancang River Embankment Management Office, Haining 314400, China; 13867363305@163.com
* Correspondence: luo810317@sohu.com; Tel.: +86-13758373234

Abstract: Due to the molding-free property and dry shrinkage of extrusion-based three-dimensional printable concrete (3DPC), the precision issues of 3DPC have not been solved effectively. One of the viable solutions for 3DPC precision improvement is to print using ultra-thin filaments. The challenges of ultra-thin-filament printing are extrudability, flowability, and fast solidification. To overcome these challenges and enhance precision, a customized 3D concrete printer with an ultra-thin diameter nozzle (6 mm) and fully sealed extrusion system was developed, and the mix design of ultra-thin-filament 3DPC (UTF-3DPC) was studied, including ingredients such as fly ash (FA), silica fume (SF), ordinary Portland cement (OPC), sodium dodecyl sulfate and cellulose (SDSC), water reducer, water, and sand. The function of UTF-3DPCs flowability and fast solidification with the proportion of water and SDSC was explored to obtain the optimal mix design. The standard compressive and flexural strengths of UTF-3DPC specimens were compared with the mold-cast vibrated and the mold-cast non-vibrated concrete. Their meso-scale and micro-scale structures were analyzed to expose the strength mechanism, according to the scanning electron microscope (SEM) images. A suitable mix design of UTF-3DPC was obtained and UTF-3DPC strength reached 80% of standard mold-cast concrete. The findings reported here provide a pathway to improve the precision of 3DPC and extend the application of 3D printing technology in engineering.

Keywords: 3D printable concrete; ultra-thin filaments; flowability; fast solidification; strength; microstructure

check for updates

Citation: Shen, J.; Li, Y.; Zhang, X.; Li, Y.; Huang, C.; Luo, W. Three-Dimensional Printable Concrete by an Ultra-Thin Nozzle and Fully Sealed Extrusion. *Buildings* **2024**, *14*, 1958. https://doi.org/10.3390/buildings14071958

Academic Editor: Peiyu Yan

Received: 19 May 2024
Revised: 19 June 2024
Accepted: 25 June 2024
Published: 27 June 2024

Copyright: © 2024 by the authors. Licensee MDPI, Basel, Switzerland. This article is an open access article distributed under the terms and conditions of the Creative Commons Attribution (CC BY) license (https://creativecommons.org/licenses/by/4.0/).

1. Introduction

3D printed concrete (3DPC) has been increasingly applied in the construction of under-5-story houses [1,2], post-tensioned segmental bridges [3,4], facilities in gardens or parks [5,6], complex templates [7], etc. worldwide. Engineering applications of 3DPC benefit us with intelligent fabrication [8], being molding-free, less labor and material consumption [9], being eco-friendly [10,11], etc. However, some barriers still hinder extensive applications in civil engineering, such as lack of reinforced concrete printing, full-graded concrete printing, and quality standards/specifications. Especially, we lack a series of standards or specifications to evaluate the precision, strength, durability, and anti-crack ability of 3DPC products including indoor, on-site experimental, and real-scale structures.

Among those issues, the precision of extrusion-based 3DPC is a non-negligible factor for structural security and integrity, which is mainly influenced by the configuration of the printer, such as filament, nozzle size, XYZ motion systems accuracy, and too significant dry shrinkage. Generally, filament or nozzle size is the primary factor for precision and surficial flatness. As shown in Figure 1, the thicker filament causes inevitable voids and surficial unevenness. The thinner the filament or nozzle is, the higher precision is and the

better surficial flatness. Usually, the thinner the nozzle and filament are, the worse the extrudability of the concrete slurry has.

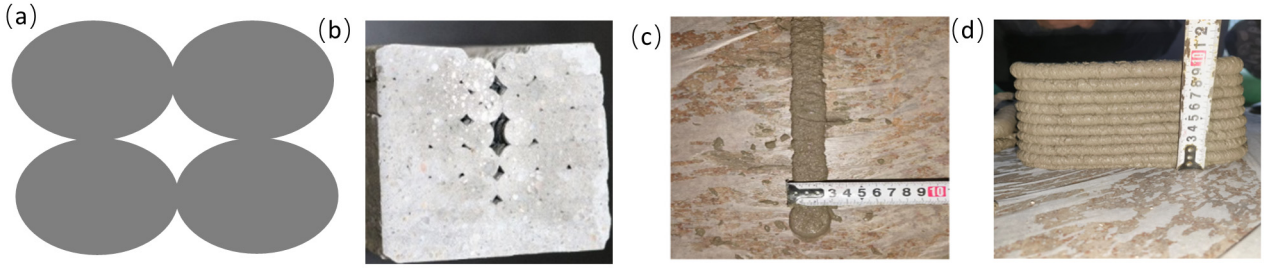


Figure 1. Void may occur during path planning (**a**), and void appears during actual printing (**b**). A 15 mm size is used for printing; the extrusion width changes to 25 mm (**c**). The designed layer height is 105 mm, and the actual layer height is 100 mm (**d**).

As shown in Table 1, current research based on printers with larger than 10 mm nozzles has been mostly reported. One exceptional example is cement-based materials printing by a printer with a 1.63 mm nozzle [12], where the aggregates are absent. There are few reports that the concrete printer with smaller than 10 mm nozzle succeeded in the research community, because the concrete slurry is hard to be extruded out continuously and fast solidify in a short time by a printer with thinner than 10 mm diameter nozzle, even though these admixtures, such as nano attapulgite clay [13], sodium carboxymethyl cellulose water-soluble polymer powder [14], hydrous magnesium aluminosilicate nanoclay [10], kaolinite clay [15], nano clay [16], cellulosic materials [17], polyacrylamide aqueous solution [18], are doped in to increase viscosity and reduce the yield stress. However, too small yield stress will reduce the buildability of 3DPC. Yield stress and viscosity are used to define the flowability of 3DPC. Besides the flowability, the fast solidification is also important for 3DPC. After extrusion, the deposited slurry should have sufficient strength to support the continuously constructed layer without excessive deformation or damage.

Table 1. Print nozzle diameter and research contents used by other researchers.

Author	The Size of Nozzle	Research Results
Bai, G., et al. [11]	30 mm	Explore the feasibility of eco-friendly concrete
Li Wang, et al. [19]	38 mm	Explore high belite sulfoaluminate and medium-heat Portland cements for large-scale 3D printing
Ma, et al. [20]	10 mm	Interlayer reinforcement in the process of printing.
L. Wang, et al. [21]	12 mm	Realize the real-time quantification of fresh and hardened mechanical property for 3D printing material
Jay G. Sanjayan, et al. [22]	25 × 10 mm rectangle	Explore the effect of surface moisture on inter-layer strength of 3D printed concrete
T.T. Le, et al. [23]	9 mm	Research on the hardened properties of high-performance printing concrete
A. Perrot, et al. [24]	35 mm circular nozzle and 21 × 42 mm rectangular nozzle	Assess the possibility of adapting the 3D printing technique to earth-based material.
Suvash Chandra Paul, et al. [25]	10 × 20 mm rectangular nozzle and 8 mm diameter nozzle	Explore the fresh and hardened properties of 3D printable cementitious materials for building and construction
Jian Hui Lim, et al. [26]	13 × 30 mm rectangular nozzle	Research on flexural characteristics of 3D printed geopolymer composites with in-process steel cable reinforcement

Table 1. *Cont.*

Author	The Size of Nozzle	Research Results
Biranchi Panda, et al. [27]	20 × 20 mm square nozzle and 15 × 30 mm rectangular nozzles.	Measurement of tensile bond strength of 3D printed geopolymer mortar
G. Ma, et al. [28]	8–30 mm nozzle	Printable properties of cementitious material containing copper tailings
Arun R. Arunothayanet, et al. [10]	30 mm nozzle	Digital fabrication of eco-friendly ultra-high performance fiber-reinforced concrete
Shin Hau Bong, et al. [5]	30 mm nozzle	Ambient temperature cured 'just-add-water' geopolymer for 3D concrete printing applications
Panda, B., et al. [13]	30 × 15 mm	Improving the 3D printability of high volume fly ash mixtures via the use of nano attapulgite clay
Sadegh Ghourchian, et al. [29]	150 × 50 mm	Modelling the development of capillary pressure in freshly 3D-printed concrete elements
Chao Liu, et al. [30]	20 mm nozzle	Influence of hydroxypropyl methylcellulose and silica fume on stability, rheological properties, and printability of 3D printing foam concrete
Nan Zhang, et al. [31]	240 mm nozzle	Short-duration near-nozzle mixing for 3D concrete printing
Bing Lu, et al. [32]	25.4 mm nozzle	Effect of printing parameters on material distribution in spray-based 3D concrete printing
Brahim Mazhoud, et al. [33]	21 × 40 mm^2 rectangular nozzle	Underwater 3D printing of cement-based mortar
Lowke, D., et al. [34]	8 mm diameter nozzle	Injection 3D concrete printing in a carrier liquid

To enhance the precision of 3DPC, a customized concrete 3D printer with 6 mm diameter nozzle and fully sealed extrusion has been developed. To successfully fabricate the ultra-thin filament 3DPC (UTF-3DPC), fly ash (FA), silica fume (SF), ordinary Portland cement (OPC), sodium dodecyl sulfate and cellulose (SDSC) at an optimal ratio are introduced to mix fine aggregates and water. The flowability and fast solidification of UTF-3DPC are measured to optimize the yield stress and viscosity. The standard samples are printed by our customized printer. The compressive and flexural strengths of UTF-3DPC have been tested and compared with ordinary standard mold-cast-vibrating and mold-cast-non-vibrating specimens. To expose the printability and strength mechanism of 3DPC, SEM imaging has been conducted. In previous research [35], the impact of different printing paths on the performance of 3DPC has been studied.

2. Material, Mix Design, Fabrication, and Testing Methods

2.1. Customized Concrete 3D Printer

To attain the robust fabrication of UTF-3DPC, we have developed our customized concrete 3D printer and fabricated specimens. Our customized concrete 3D printer is characterized by an ultra-thin nozzle with the diameter of 6 mm. Its benefits include higher accuracy and better surface flatness. It consists of an entire framework, XYZ motion system, extrusion system, slurry conveying system, mainboard, and embedded operating system as shown in Figure 2a,c. The entire framework is combined by base tray and gantry crane with the size of 500 mm long, 500 mm wide, and 700 mm high. The extruder in Figure 2b is mounted on the beam in the gantry crane, which controls X and Z axis movement, while the base tray moves along the Y axis. All X, Y, and Z axes movements in the XYZ motion system are driven by stepper motors and screw rods. The extruding system is featured by the fully sealed extrusion, including the extruder, plastic tube, and material tank. The concrete slurry sealed in the material tank is propelled by the conveying system into plastic tube and extruded out through the nozzle on the extruder. The slurry conveying system includes air compressor and the piston in the material tank. The mainboard and embedded

operating system are used to control nozzle or trays moving path as given route. The maximum printing size of the specimens is 200 mm × 200 mm × 180 mm. The cylindrical material tank with an inner diameter of 50 mm is placed vertically next to the printer to ensure smooth propelling. The plastic tube with an inner diameter of 8 mm is used to deliver slurry into the extruder. An air compressor provides the high-pressure air to propel the piston at a stable velocity.

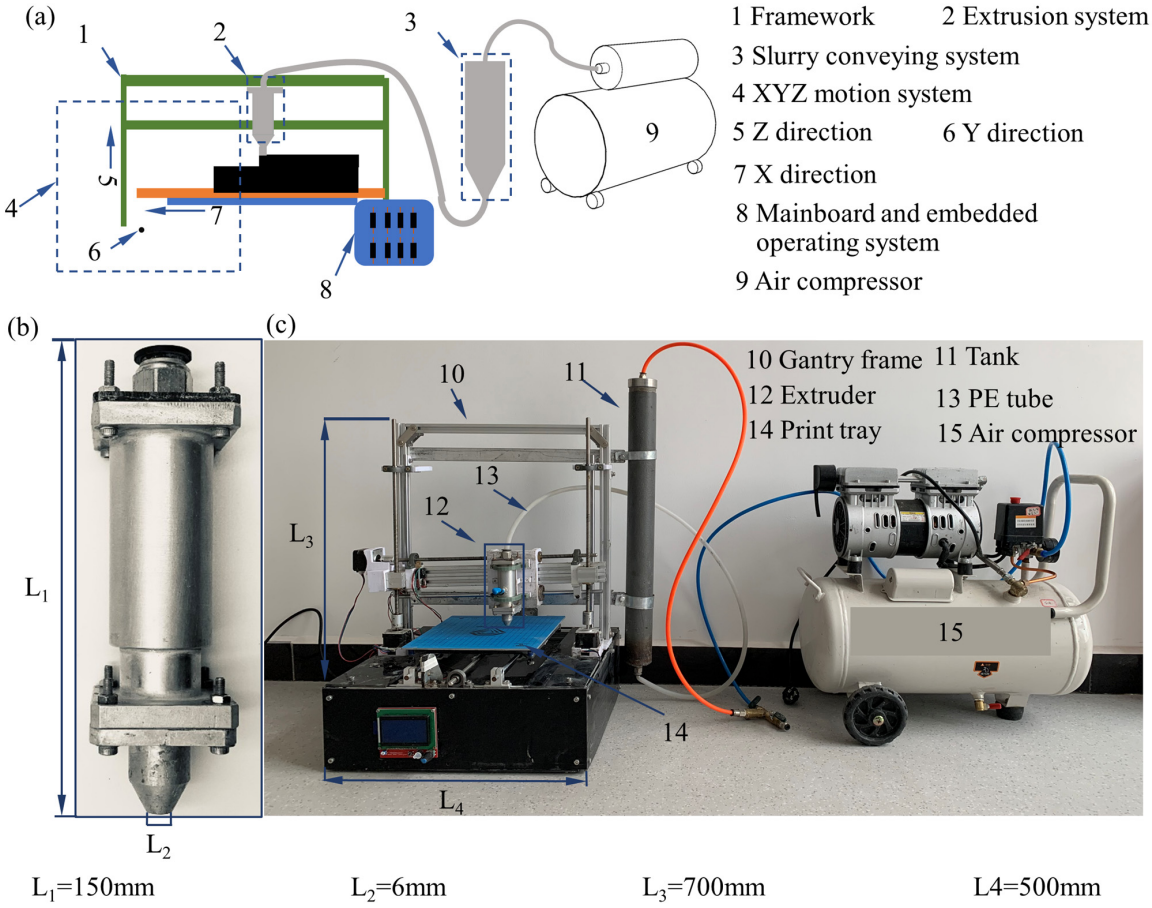


Figure 2. (**a**) The model diagram of the customized ultra-thin nozzle printer. It consists of entire framework, XYZ motion system, extrusion system, slurry conveying system, mainboard, and embedded operating system. (**b**) The extruder with 150 mm height and a 6 mm ultra-thin nozzle. (**c**) The real image of customized ultra-thin nozzle concrete 3D printer.

2.2. Materials and Mix Proportion

The optimal admixtures and mix design have been explored to ensure extruding the slurry out. To extrude the slurry smoothly, ingredients such as fly ash (FA), silica fume (SF), ordinary Portland cement (OPC), sodium dodecyl sulfate, and cellulose (SDSC) at a certain ratio are introduced to mix natural sand, water reducer, and water, and to fabricate the concrete specimens. The SEM images of the main ingredients are shown in Figure 3. The magnitude of 1000 times witnesses 2–10-micron spherical particles of FA in Figure 3a. SF behaves as 200–500-nanometer spherical particles in Figure 3b, while OPC as angular particles with the size of 1–50 micron in Figure 3c, and SDSC as angular particles with the size of 10–50 microns as well as fiber of 30 microns long in Figure 3d. The natural sand ranges from 0.08 mm to 2 mm.

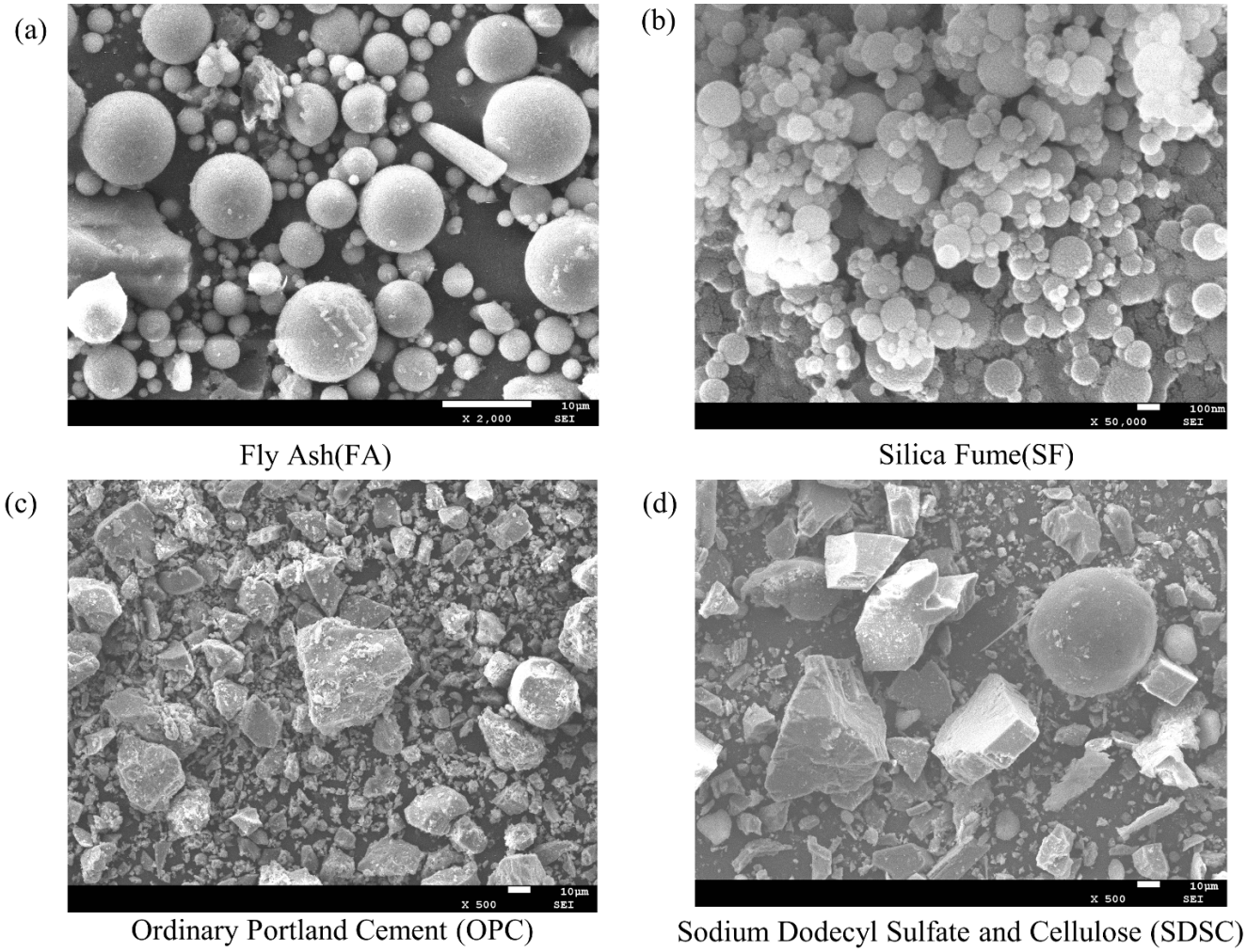


Figure 3. SEM images of such main ingredients as (**a**) FA, (**b**) SF, (**c**) OPC, and (**d**) SDSC.

As a supplementary material for OPC, FA hydrates together with OPC, and adheres other ingredients and aggregates. Since the nozzle diameter of the customized concrete 3D printer is smaller than the nozzle diameters mentioned in most papers, more attention needs to be paid to the study of the extrudability and flowability of the concrete slurry. To be extruded smoothly, SF and SDSC are introduced to reduce the shear force between particles and the friction of the slurry and the nozzle or pipe. Also, SDSC is employed as a water-retaining material to lock the water inside the slurry under high pressure and avoid bleeding water out of the slurry. SDSC carrying water also feeds cementitious material with water to extend the hydration process. As for the admixture, polycarboxylic acid high-performance water-reducing agent is used as water reducer to control the workability of the slurry. After previous research [35] and experiments, the ratio of fine aggregates and cementitious materials is set to approximately 0.5. To explore optimal water or SDSC, six mix designs include W550SDSC14, W600SDSC14, W650SDSC14, W600SDSC7, W600SDSC14, and W600SDSC21 as shown in Table 2.

The chemical composition of the materials used is identical to that used in previous research [35].

Table 2. Mix ratios design of flowability test (kg/m^3).

Mix Ratios Design	Water	OPC	FA	SF	Sand	Water Reducer	SDSC
W550SDSC14	550	800	400	50	800	0.12	14
W600SDSC14	600						14
W650SDSC14	650						14
W600SDSC7	600	800	400	50	800	0.12	7
W600SDSC14	600						14
W600SDSC21	600						21

2.3. Specimen Fabrication

According to mix designs, all ingredients are put together, stirred evenly to obtain the slurry. Then the slurry is infused into the cylindrical tank. Before being sealed in the tank, air in the pipe and tank should be discharged out to ensure continuous extrusion. After 3D models of specimens are sliced into layers and filaments as shown in Figure 4a, printing paths from bottom to top are generated, which guide the nozzle to move and simultaneously extrude slurry out at a certain velocity under high-pressure air produced by air compressor. As shown in Figure 4b, 6 mm-diameter filaments are stacked into a layer. After stacking the current layer, the nozzle will move upward 5 mm to print a new layer until the specimen in Figure 4c is printed out. To print concrete specimens smoothly, 6 mm diameter filament or nozzle and 30 mm/s of nozzle moving velocity have been finally adopted. Every single printing layer is 5 mm high. The infill density is set as 100%. The air pressure of delivering the slurry is set as 0.4 MPa.

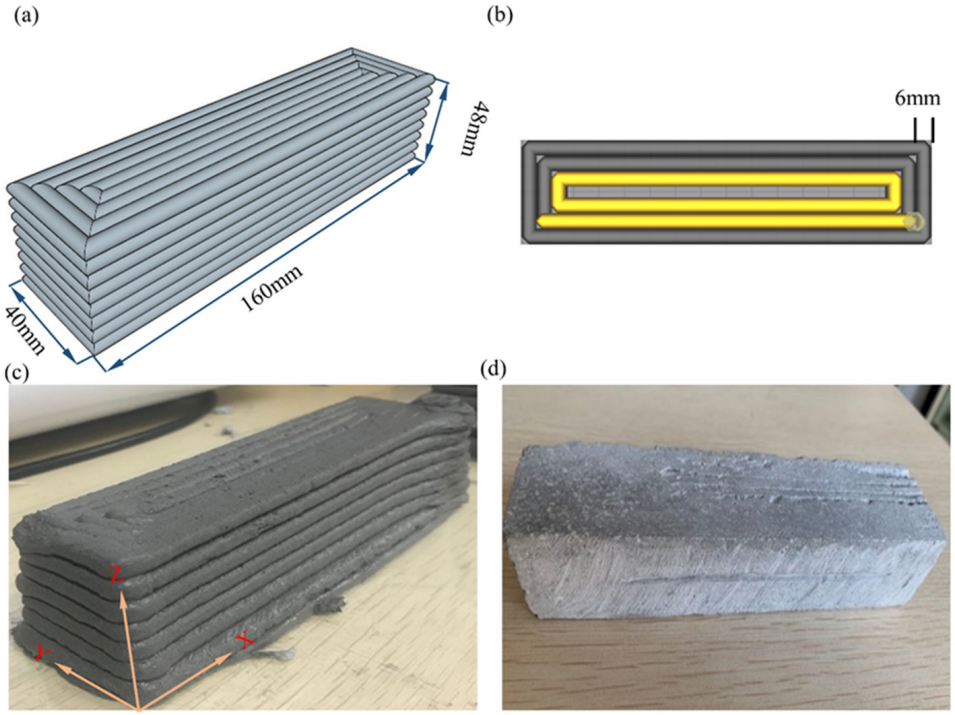


Figure 4. The sliced 3D model (**a**), filaments in a layer (**b**), printed specimen (**c**), and polished specimen of UTF-3DPC (**d**).

After curing for 28 days in a standard thermal and humid environment, specimens are polished into standard concrete specimens (40 mm × 40 mm × 160 mm), as shown in Figure 4d.

2.4. Flowability and Fast Solidification Testing

2.4.1. Flowability

According to multiple standards, GB/T 2419-2005 [36], several methods are introduced to test the flowability of concrete slurry, including the consistometer [5,11] and flow table test [11,28]. The consistometer is used here because the penetrating cone bears friction and resistance of the concrete slurry, which is similar to 3DPC.

During the experiment, the mixed mortar was placed in the consistometer, and the depth of the cone barrel of the consistency instrument was 150 mm. The mortar inside the cone barrel was punctured and the depth that the cone punched can be measured in the consistency. By this method, the performance of the mortar with different mix ratios is tested first, and the material performance is evaluated and printed after the relevant data is obtained.

Flowability plays a significant role in 3DPC. During the 3D printing process, concrete requires a lower yield stress and an appropriate plastic viscosity. The yield stress is computed from the depth of penetration h of the standardized cone used in this study (tip angle θ = 30°, mass of m = 300 g) as Equation (1) [33]:

$$\tau_0 = \frac{m \times g \times cos^2\theta}{\pi h^2 \times tan\theta} \quad (1)$$

where g is the gravity acceleration.

The dosage of water and the amount of SDSC are the main factors which affect the flowability. Because the printer nozzle is ultra-thin (6 mm), even a small change in the amount of water will have a great impact on the flowability of the slurry. As shown in Table 1, 5 mix designs are adopted according to the controlled variable method. To find out optimal water or SDSC proportion, mix designs W550SDSC14, W600SDSC14, and W650SDSC14 take water as variable floating ±50 g, and mix designs W600SDSC7, W600SDSC14, W600SDSC21 take SDSC as variable floating ±7 g. Three specimens are made in the same mix design.

2.4.2. Fast Solidification

According to ASTM GB/T 2419-2005, the velocity of solidification is depicted by the time of initial solidification, which is tested by the penetrometer. For successful printing, the materials used in 3DPC should be continuously extruded through the nozzle without any blockage or segregation. After extrusion, the deposited material should have sufficient strength to support the continuously constructed layer without excessive deformation or damage.

2.5. Strength Testing

To investigate the hardened properties, the flexural and compressive testing have been carried out. The distance between the two support columns in the flexural testing is taken as 100 mm. Flexural strength is calculated according to Equation (2). After the flexural test, two specimens are generated for compressive test with a compressive area of 40 × 40 mm. The arithmetic mean value of the measured flexural strength of three specimens in each group is taken.

$$f_{ts} = \frac{2\mathrm{P}}{\pi A} = 0.637\frac{P}{A} \quad (2)$$

The compressive strength is calculated as

$$f_{cc} = \frac{P}{A} \quad (3)$$

where f_{ts} is the splitting tensile strength (MPa), P is failure load (N), A is specimen split surface area (mm^2), and f_{cc} is compressive strength (MPa).

2.6. SEM Imaging

To expose the strength mechanism of UTF-3DPC, the microstructures of concrete are imaged by SEM scanning. The instrument for SEM pictures is JSM-7500F scanning electron microscope produced by Japan Electronics Corporation. The software, Image-Pro Plus 6.0, is used to analyze the porosity of specimens. This software can perform pixel analysis based on the microscopic images.

3. Results and Discussion

By means of the controlled variable method, the optimal mix design of UTF-3DPC is obtained. UTF-3DPCs flowability, fast solidification, strength, and microstructure are evaluated. The precision of 3DPC has been effectively enhanced by ultra-thin filament.

3.1. Flowability

To find out the optimal flowability, the penetration resistance and yield stress of 5 mix ratios of UTF-3DPC have been measured as shown in Figure 5. Comparison of the yield stress of W550SDSC14, W600SDSC14, and W650SDSC14 shows that the yield stress decreases continuously from 387 Pa to 124 Pa as the dosage of the water increases as shown in Figure 5f. Also, as the dosage of SDSC increases continuously from 7 g to 21 g, the yield stress decreases from 248 Pa to 144 Pa as shown in Figure 5f. The yield stress of W600SDSC14 is 185 Pa, which is in the middle of all UTF-3DPC. Generally, the appropriate yield stress ensures UTF-3DPC being extruded continuously and robustly. Extrusion testing proves that 185 Pa is the best yield stress for UTF-3DPC, which is less than 250.2 Pa of 30 mm-rectangular-nozzle 3DPC [5], but it is contained in 66–230 Pa of 20 mm-circular-nozzle 3DPC [30].

From Figure 5f, it can be seen that with the increase in water dosage from 550 to 600, the water dosage only increased by 50, but the yield stress decreased by 31%. As the yield stress decreased, the flowability gradually increased, indicating that with an increase in the water content, the flowability gradually increased, but it is important to note that the flowability may affect the printing quality. The reason is that the incorporation of water makes the adhesion force between the various components of the 3DPC become worse, and it is not so easy to gather into groups.

As a water retaining agent, SDSC can reduce the water loss to a certain extent and promote the flowability, especially when extrusion-based UTF-3DPC slurry is compressed by air pressure. The absence of SDSC always causes water to seep out of UTF-3DPC slurry under the air pressure. The most important function of SDSC is to increase the water retention of concrete and make the slurry be extruded smoothly. Therefore, it is necessary to strictly control the water consumption and the amount of SDSC during the experiment to achieve a balance between the flowability and fast solidification of concrete.

3.2. Fast Solidification

The solidification results of the experiment are shown in Figure 5. The horizontal dashed line in Figure 5a–e represents the penetration resistance of 3.8 MPa, which corresponds to the initial setting time of the printing material. The solidification time curves of five different mix ratios of concrete have been fitted, respectively. It is indicated that they are all approximately in line with the relationship of exponential functions such as $y = Ae^{Bx}$. It can be seen that the amount of water is dominating in the entire solidification testing process.

From Figure 5, it can be seen that as water dosage gradually increases, the slope of the curve gradually decreases, which means that the hardening rate of 3DPC gradually decreases, which is in line with expectations. However, for the increase in the amount of SDSC used, its effect of enhancing early strength and accelerating hydration reactions is not as significant.

The late solidification means that sufficient strength cannot be obtained in the early stage to support the printing of subsequent layers. On the contrary, too early solidification

causes the decrease of the adhesive strength between the previous layer and the subsequent layer, which is also an unfavorable factor for constructability. So, either too early or late solidification results in UTF-3DPC tilting or even collapsing during the printing process. The initial setting time of our proposed UTF-3DPC is about 8 h, which is much longer than the solidification time of other larger-filament printers [5].

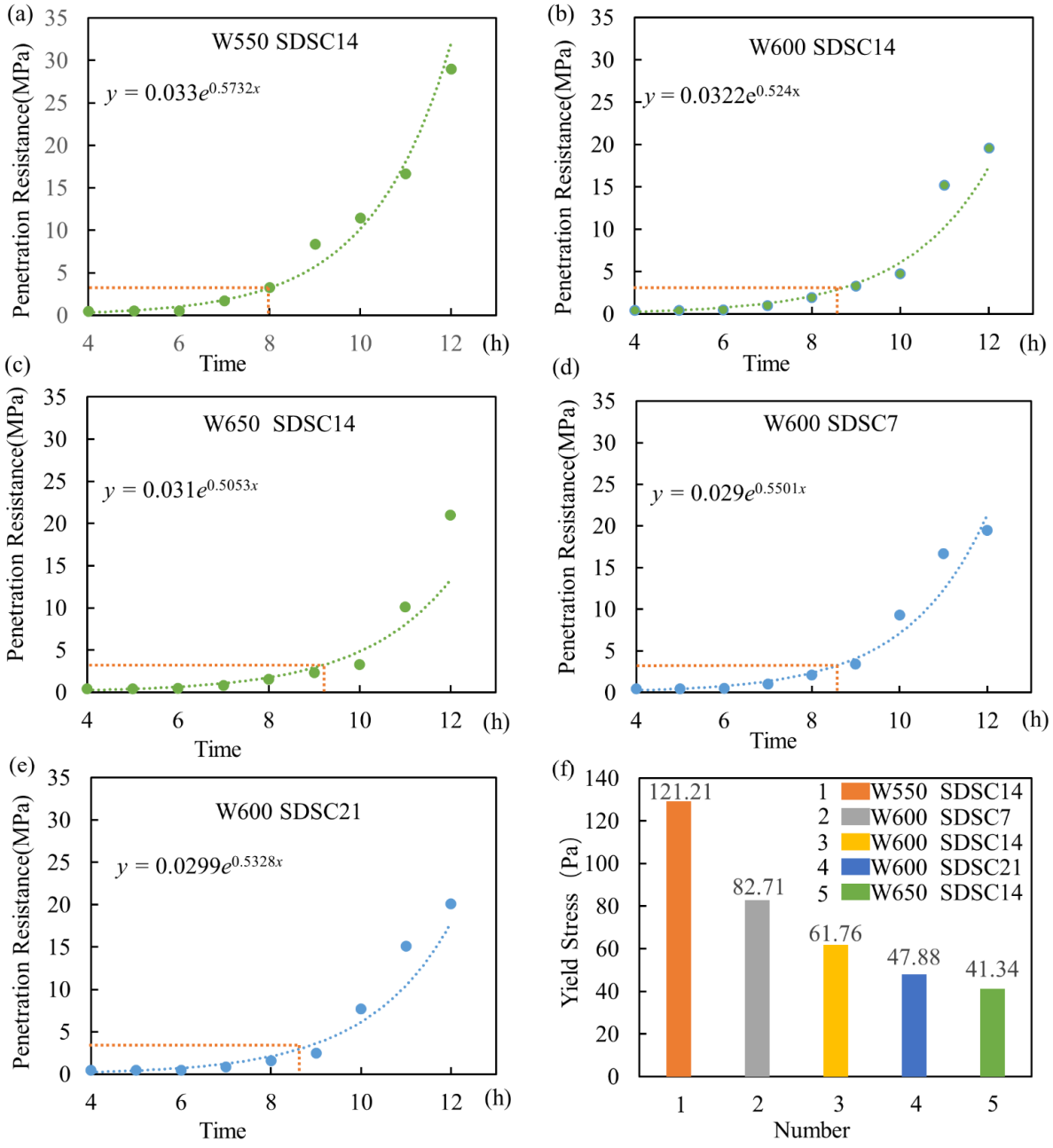


Figure 5. Comparison of fast solidification and flowability data under five different mix ratios. (**a**) W550 means adding water 550 mL, SDSC7 means adding SDSC 7 g, (**b**) W600 means adding water 600 mL, SDSC14 means adding SDSC 14 g, (**c**) W650 means adding water 650 mL, SDSC14 means adding SDSC 14 g, (**d**) W600 means adding water 600 mL, SDSC7 means adding SDSC 7 g, (**e**) W600 means adding water 600 mL, SDSC21 means adding SDSC 21 g. (**f**) The flowability data of printing materials with different mixing ratios.

3.3. Printability Evaluation

Extrudability is a comprehensive manifestation of flowability and rapid solidification. The satisfactory extrudability is manifested by uniform discharge, no clogging, and excessive discharge. When a pressure of 2 bar was applied, the granular slurry cannot be continuously extruded out due to too low air pressure or too dry slurry. Appropriate water, spherical SF and FA, and SDSC are introduced to increase flowability. When 5 bar air pressure is used for extrusion in the experiment process, too much slurry was extruded at one time, which caused the experiment to fail. After reducing the air pressure to 4 bar and increasing the amount of water reducing agent, the extrusion can be performed normally.

It can be seen that many attempts are needed in the process of using the technology of full seal extrusion, and different material properties need different technical parameters to improve the printing quality. Compared with direct extrusion, the construction process of full seal extrusion is more complex, but to some extent, it can improve printing accuracy.

In the experiment, it was found that the printing effect is the best when the yield stress is 50 Pa to 65 Pa through observation and measurement. As can be seen from Figure 6, the relevant data of the fitting curve can be used to obtain the best water consumption and the best dosage of SDSC for the best printing effect. The percentages mentioned here refer to the ratio of SDSC and water to the absolute mass of the cementitious material.

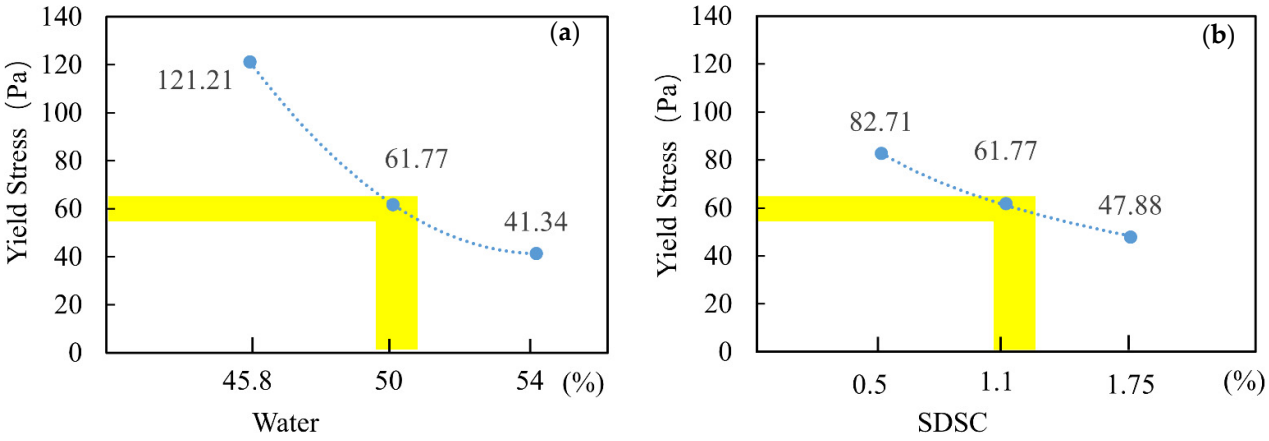


Figure 6. The (**a**) Change in yield stress with changes in water consumption curve and (**b**) change in yield stress with changes in SDSC consumption curve.

In fact, in ordinary 3DPC of larger than 10 mm nozzle, the extrusion is just used to deliver the concrete slurry from material tank to pump hopper, while printing is attained by self-gravity of the slurry and auger force. The extruder of our UTF-3DPC printer does not include pump hopper and the auger, because the pump and auger disturb the sealed slurry, which causes failure of printing process. Many attempts prove that fully sealed extrusion guarantees smooth printing.

3.4. Opening Time and Printing Speed

To obtain optimal printing speed, the printing speeds of 10 mm/s, 30 mm/s, and 50 mm/s were used. Table 3 summarizes the extrudability and buildability parameters of the mixtures printed at different speeds. The successful extrudability and buildability are denoted as 'Y', while the failures are denoted as 'N'.

The main difficulty encountered in the printing process is that extrusion-based 3DPC needs to match the printing speed and extrusion speed; otherwise, cracks, breaks, or accumulations occur. When the slurry is extruded out at 10 mm/s printing speed, the slurry accumulates, while at a speed of 50 mm/s, the slurry bears excessive tension and becomes discontinuous.

Table 3. Evaluation of extrudability and buildability of the mixtures.

Print Speed (mm/s)	W550 SDSC14	W600 SDSC14	W650 SDSC14	W600 SDSC7	W600 SDSC21
10	N/N	Y/N	Y/N	Y/N	Y/N
30	N/N	Y/Y	Y/N	Y/N	Y/Y
50	N/N	Y/N	Y/N	Y/N	Y/N

Note: Y/Y denotes successful extrudability/buildability; Y/N denotes successful extrudability but unsuccessful buildability.

3.5. Strength Analysis

Because the common compressive and flexural directions of concrete are in the Z direction, the specimens of the three different molding methods are all carried out in the Z direction. Under the above mix ratios (Table 1), three types of specimens have been produced, namely printing, mold-cast-vibrating, and mold-cast-non-vibrating. The average compressive strengths of these three in Figure 7a are 20.1 MPa, 31.6 MPa, and 22.35 MPa, respectively. Compared with the mold-cast-vibrating specimens of the same mix ratio, the compressive strengths of the printed and mold-cast-non-vibrating specimens decrease by 36% and 29%, respectively. The average flexural strengths of these three types are 4.54 MPa, 5.98 MPa, and 4.92 MPa, respectively. The printed and mold-cast-non-vibrating specimens are 24% and 17.7% lower than the mold-cast-vibrating specimens. Compressive and flexural strength loss of the printed specimens result from relatively loose bonding between the middle filaments, as shown in Figure 8a, which is mainly due to the fact that 40 mm width of specimens is not exactly divided by 6 mm of filaments.

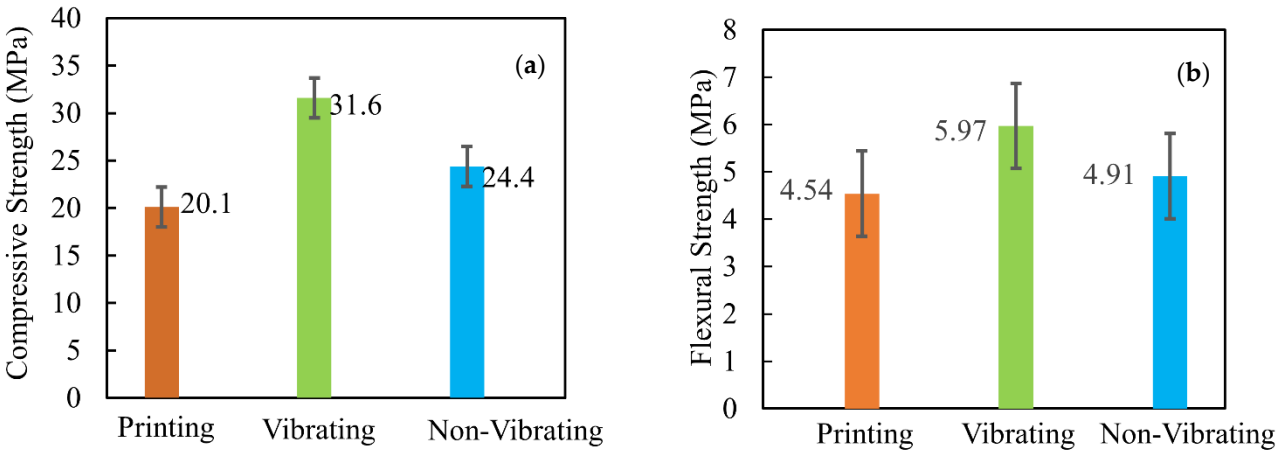


Figure 7. Comparison of compressive (**a**) and flexural (**b**) strengths of specimens with the same mix ratio and different molding methods. *Printing* represents printed specimens. *Vibrating* represents mold-cast-vibrating specimens. *Non-Vibrating* represents mold-cast-non-vibrating specimens.

From the perspectives of flexural strength and compressive strength, there appears to be a significant gap, which is due to the obvious anisotropy of 3DPC, meaning that there are significant differences in strength in the X, Y, and Z directions during strength testing. During flexural strength testing, the combination bending strength of multiple printed filaments is measured until all filaments have broken, at which point the entire specimen is completely destroyed. For compressive strength testing, during the experiment, due to possible gaps between the filaments, individual filaments may crack, at which point the experimental equipment recognizes the damage and stops testing, only measuring a filament of the strength. This is also one of the reasons why printed specimens have significantly lower strengths compared to cast specimens.

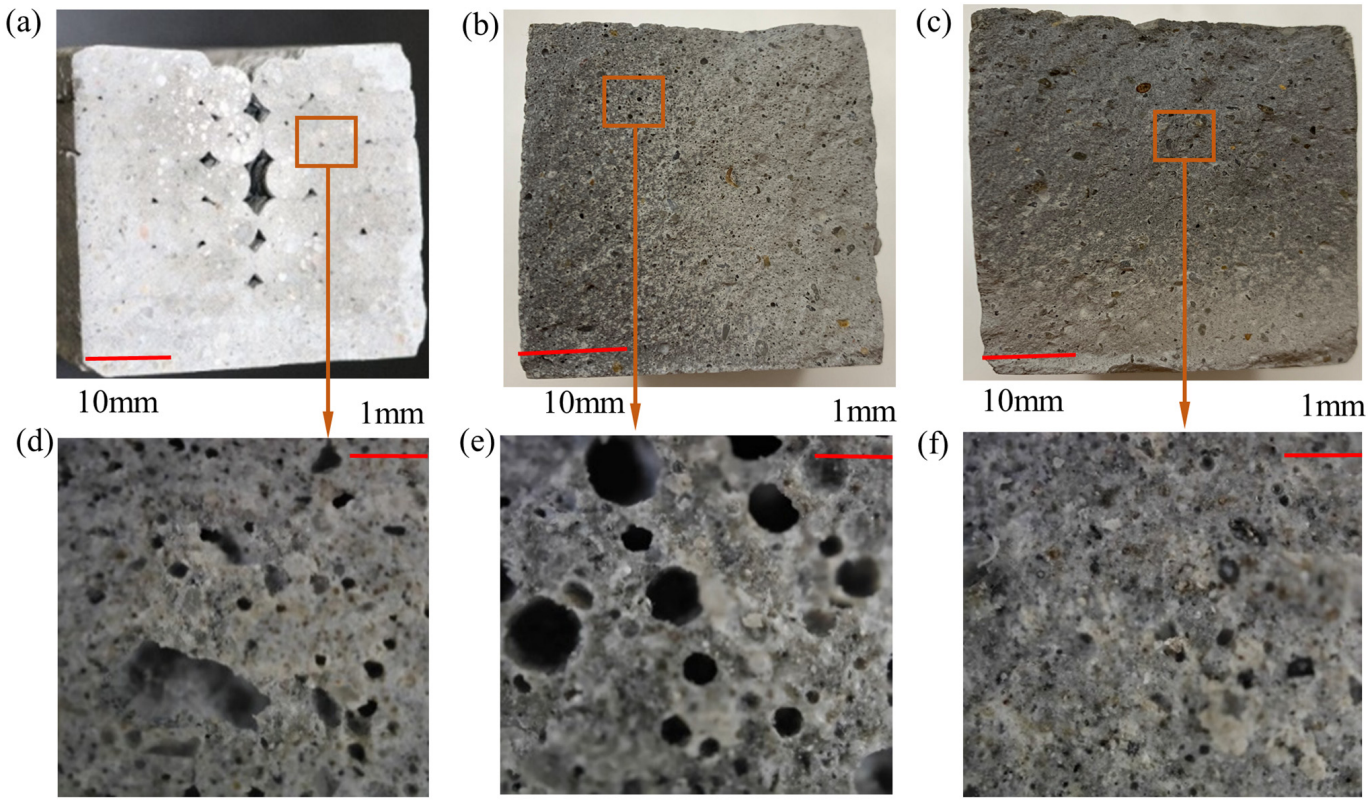


Figure 8. (**a**,**d**) are the cross-section and meso-scale view of the printed specimen. (**b**,**e**) are the cross-section and meso-scale view of the mold-cast-non-vibrating specimen. (**c**,**f**) are cross-section and meso-scale view of mold-cast-vibrating specimen.

3.6. Porosity Analysis

As shown in Figure 8a–c, macro-scale comparison of printing, mold-cast-non-vibrating, and mold-cast-vibrating specimens cross section shows that mold-cast-non-vibrating and mold-cast-vibrating specimens present more uniformly distributed porosity structures than printed ones. Obvious voids occur in the printed specimen. Down to meso-scale level, in Figure 8d,e, printing and vibrating specimens possess smaller pores than non-vibrating, which is proved by the statistics on the total porosity area and proportion in Figure 9a. The largest macro-scale porosity of the printed specimen is due to the fact that 40 mm width of the specimen is not exactly divided by 6 mm width of the filament, which causes inborn void in the middle section. Consequently, the voids weaken the strengths of the printed specimen. The meso-scale picture of the printed specimen is taken in the filament section. Because our UTF-3DPC is compressed dense in the material tank, the compressed slurry is denser than mold-cast-vibrating and mold-cast-non-vibrating. As soon as the voids between filaments are solved, the UTF-3DPC is more promising style than traditional construction.

According to Figure 9b–d, various porosities are evenly distributed in three specimens. But pore sizes of the printed specimen range from 0.1 to 0.4 mm, the mold-cast-non-vibrating 0.04 to 0.8 mm, and the mold-cast-vibrating 0.01–0.08 mm, which also confirms that the strength of the mold-cast-vibrating specimen is the best among these three.

However, it should be noted that during the process of porosity analysis, only a portion of the image is selected for analysis, and the most characteristic image is used to demonstrate the different effects brought about by different forming methods. Differences in other sectional specimens can be further explored through X-ray scanning.

Further down to micro-scale level, comparison between micro-scale images of these three indicates that calcium silicate hydrate (C-S-H) effectively adheres to SF, FA, SDSC, and sand in Figures 10–12. C-S-H, which is a gel-like substance formed after cement hydration

reaction, can be well distinguished in micro-images. FA, as a supplementary cementing material, presents as round balls, while SF acts as a lubricant to reduce shear force between various components, which facilitates better extrudability of the material. But the existence of voids and cracks in different sizes and proportions results in the different macro-scale strength of these three specimens. As shown in Figures 10a, 11b and 12b, the printed and the mold-cast-vibrating specimens are denser than the mold-cast-non-vibrating. Due to the compressing action of the piston, the UTF-3DPC has the approximate density as the mold-cast-vibrating specimen. If the bad adhesion between filaments is improved, the strength of the printed specimen will reach the strength of the mold-cast-vibrating specimen.

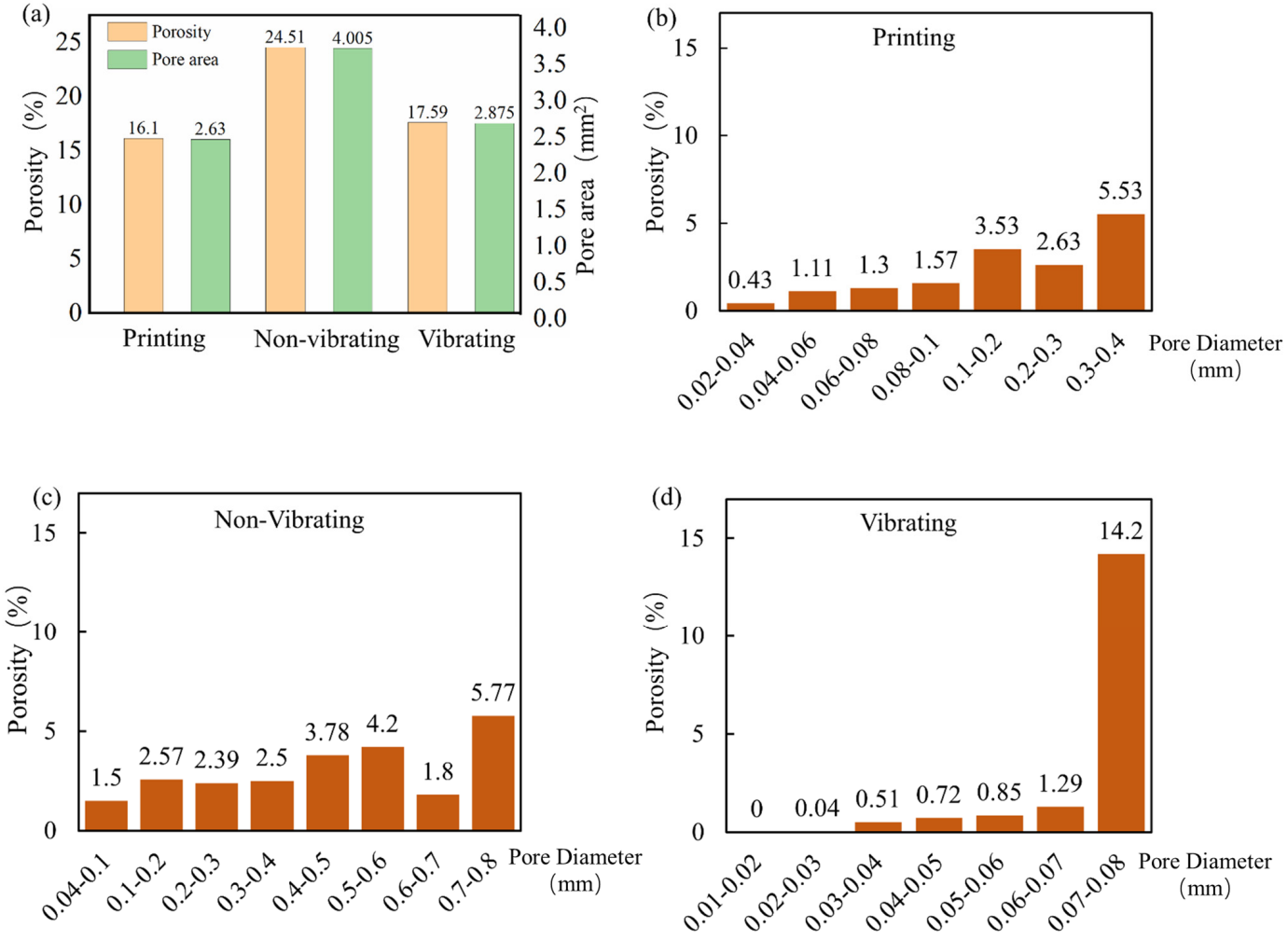


Figure 9. Comparison of porosity of specimens made by three different methods. (**a**) The total porosity and pore area of the specimens. (**b**) is the pore distribution of the printed specimen. (**c**) is the pore distribution of the mold-cast-non-vibrating specimen. (**d**) is the pore distribution of the mold-cast-vibrating specimen.

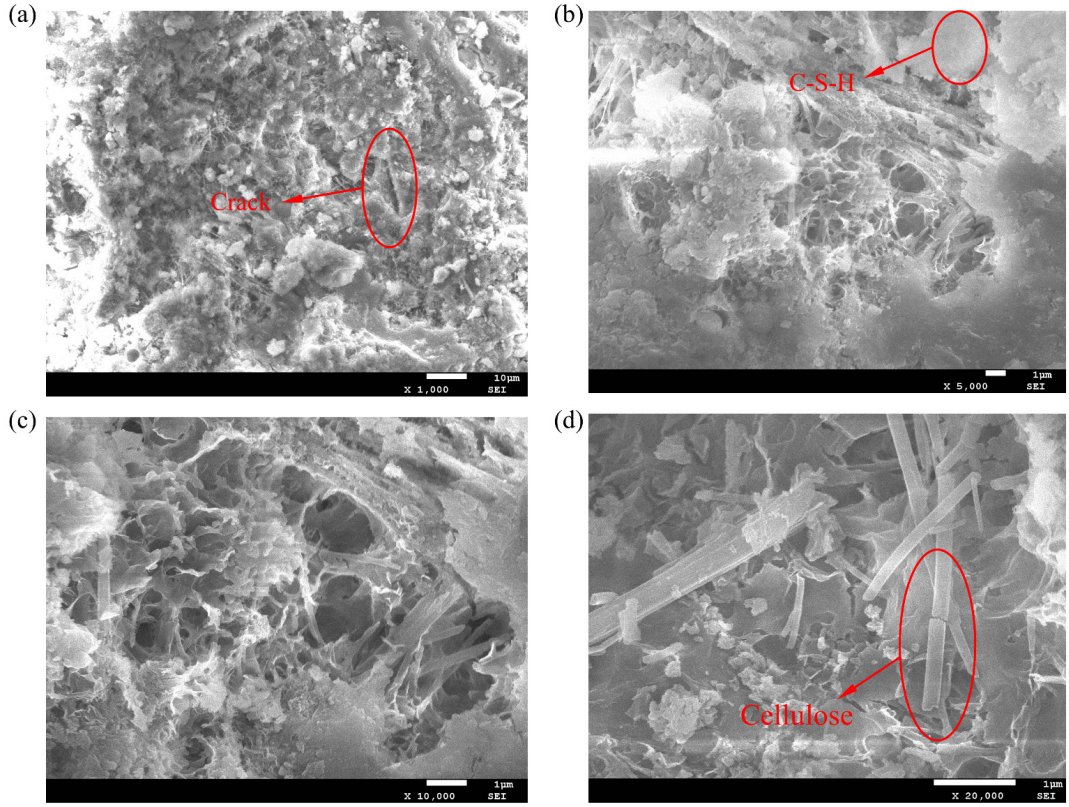


Figure 10. 1000 (**a**), 5000 (**b**), 10,000 (**c**), and 20,000 (**d**) times magnified SEM images of printed specimens.

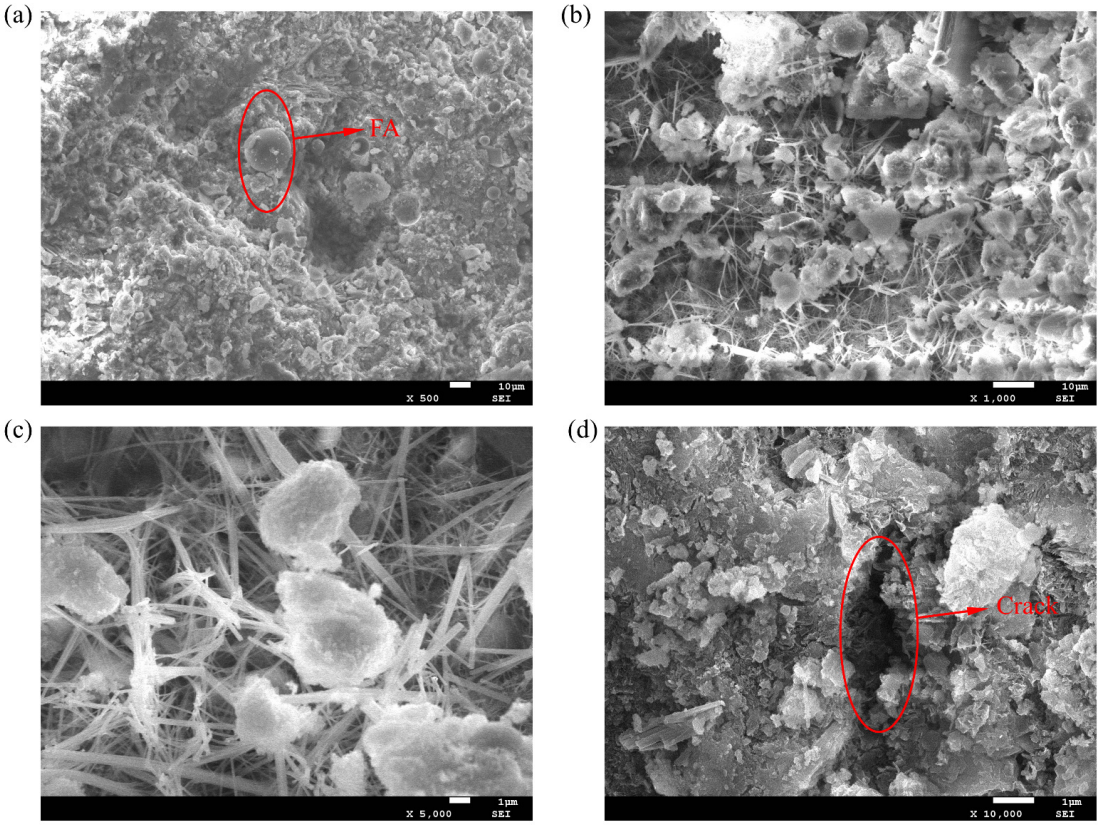


Figure 11. 500 (**a**), 1000 (**b**), 5000 (**c**), and 10,000 (**d**) times magnified SEM images of mold-cast-non-vibrating specimens.

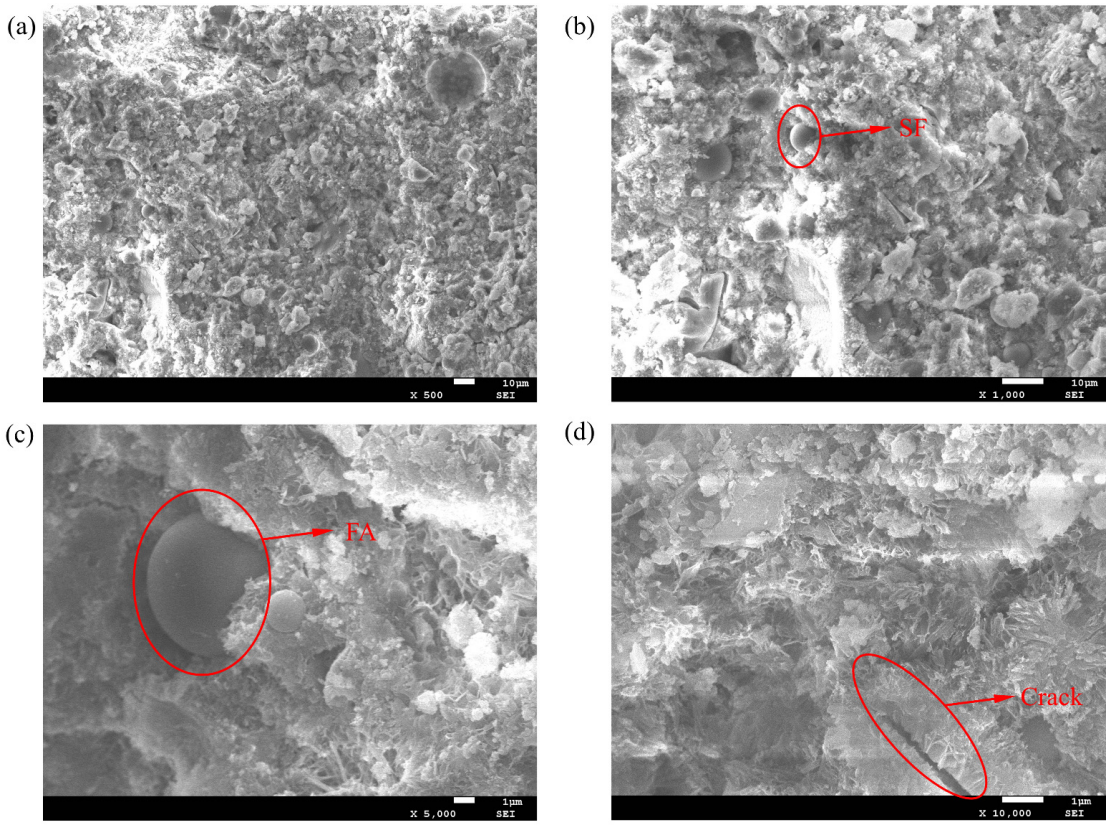


Figure 12. 500 (**a**), 1000 (**b**), 5000 (**c**), and 10,000 (**d**) times SEM images of the mold-cast-vibrating specimens.

4. Conclusions

To improve the precision of 3DPC, the ultra-thin filament 3DPC (UTF-3DPC) is proposed and a customized concrete 3D printer with 6 mm circular nozzle and fully sealed extrusion system is developed. To obtain optimal flowability, extrudability, and fast solidification of UTF-3DPC, FA, SF, SDSC, and water reducer are introduced to mix with OPC, water, and sand in different proportions. To obtain the optimal mix ratio, the yield stress, the penetration volume, and the initial setting time of UTF-3DPC of different mix ratios are measured according to the standard methods. Optimal mix ratio, appropriate printing and extruding speed, and air pressure ensure succeeding the fully sealed UTF-3DPC printing. To verify the practicability of UTF-3DPC, the compressive and tensile strengths of UTF-3DPC are compared with mold-cast-vibrating and mold-cast-non-vibrating specimens. To explore the underlying mechanism of UTF-3DPC strength, the macro-scale, meso-scale, and micro-scale porosity structures are imaged via camera and SEM method. Some conclusions are made as follows:

1. UTF-3DPC can effectively improve print accuracy, but adjustments to printing parameters are significant during the printing process to achieve good print results;
2. The 6 mm-filament 3DPC can be printed successfully at 30 mm/s printing speed, 0.4 MPa air pressure;
3. UTF-3DPC includes FA, SF, SDSC, water reducer, sand, water, and OPC. FA and SF are helpful to optimize the gradation of UTF-3DPC. SDSC plays a key role in improving the flowability, extrudability, and printability, and retaining water under the air pressure;
4. The optimal dynamic yield stress and initial setting time of UTF-3DPC are 175 Pa to 200 Pa, and 8 h, respectively;
5. The strength of UTF-3DPC reaches 80% of mold-cast-vibrating concrete;
6. If the inter-filament adhesion of UTF-3DPC can be improved, the strength of UTF-3DPC will be further enhanced;

7. The meso-scale and micro-scale structures of UTF-3DPC indicate that air pressure is beneficial to enhance its strength due to fully sealed extrusion system. Under the air pressure, fully sealed UTF-3DPC becomes denser than mold-cast-non-vibrating concrete;
8. The findings reported here provide a pathway to improve the precision of 3DPC and extend the application of 3D printing technology in engineering.

Author Contributions: Conceptualization, J.S. and Y.L. (Yangbo Li); methodology, X.Z. and Y.L. (Yujia Li); software, J.S. and Y.L. (Yujia Li); formal analysis, W.L., X.Z. and C.H.; resources, W.L., X.Z., Y.L. (Yangbo Li) and C.H.; writing—original draft preparation, J.S.; writing—review and editing, Y.L. (Yangbo Li); supervision, W.L., Y.L. (Yangbo Li) and C.H.; project administration, W.L. All authors have read and agreed to the published version of the manuscript.

Funding: This research received no external funding.

Data Availability Statement: All relevant data are within the paper.

Conflicts of Interest: The authors declare no conflicts of interest.

List of Abbreviations in the Research

3DPC	three-dimensional printable concrete
UTF-3DPC	ultra-thin-filament three-dimensional printable concrete
FA	Fly ash
SF	Silica fume
OPC	ordinary Portland cement
SDSC	sodium dodecyl sulfate and cellulose
SEM	scanning electron microscope

References

1. Furet, B.; Poullain, P.; Garnier, S. 3D Printing for Construction Based on a Complex Wall of Polymer-Foam and Concrete. *Addit. Manuf.* **2019**, *28*, 58–64. [CrossRef]
2. Hager, I.; Golonka, A.; Putanowicz, R. 3D Printing of Buildings and Building Components as the Future of Sustainable Construction? *Procedia Eng.* **2016**, *151*, 292–299. [CrossRef]
3. Vantyghem, G.; De Corte, W.; Shakour, E.; Amir, O. 3D Printing of a Post-Tensioned Concrete Girder Designed by Topology Optimization. *Autom. Constr.* **2020**, *112*, 103084. [CrossRef]
4. Salet, T.A.M.; Ahmed, Z.Y.; Bos, F.P.; Laagland, H.L.M. Design of a 3D Printed Concrete Bridge by Testing. *Virtual Phys. Prototyp.* **2018**, *13*, 222–236. [CrossRef]
5. Bong, S.H.; Xia, M.; Nematollahi, B.; Shi, C. Ambient Temperature Cured "just-Add-Water" Geopolymer for 3D Concrete Printing Applications. *Cem. Concr. Compos.* **2021**, *121*, 104060. [CrossRef]
6. Ma, G.; Wang, L.; Ju, Y. State-of-the-Art of 3D Printing Technology of Cementitious Material—An Emerging Technique for Construction. *Sci. China-Technol. Sci.* **2018**, *61*, 475–495. [CrossRef]
7. Xiao, J.; Ji, G.; Zhang, Y.; Ma, G.; Mechtcherine, V.; Pan, J.; Wang, L.; Ding, T.; Duan, Z.; Du, S. Large-Scale 3D Printing Concrete Technology: Current Status and Future Opportunities. *Cem. Concr. Compos.* **2021**, *122*, 104115. [CrossRef]
8. Bai, G.; Wang, L.; Wang, F.; Ma, G. In-Process Reinforcing Method: Dual 3D Printing Procedure for Ultra-High Performance Concrete Reinforced Cementitious Composites. *Mater. Lett.* **2021**, *304*, 130594. [CrossRef]
9. Bhattacherjee, S.; Basavaraj, A.S.; Rahul, A.V.; Santhanam, M.; Gettu, R.; Panda, B.; Schlangen, E.; Chen, Y.; Copuroglu, O.; Ma, G.; et al. Sustainable Materials for 3D Concrete Printing. *Cem. Concr. Compos.* **2021**, *122*, 104156. [CrossRef]
10. Arunothayan, A.R.; Nematollahi, B.; Ranade, R.; Khayat, K.H.; Sanjayan, J.G. Digital Fabrication of Eco-Friendly Ultra-High Performance Fiber-Reinforced Concrete. *Cem. Concr. Compos.* **2022**, *125*, 104281. [CrossRef]
11. Bai, G.; Wang, L.; Ma, G.; Sanjayan, J.; Bai, M. 3D Printing Eco-Friendly Concrete Containing under-Utilised and Waste Solids as Aggregates. *Cem. Concr. Compos.* **2021**, *120*, 104037. [CrossRef]
12. Moini, M.; Olek, J.; Youngblood, J.P.; Magee, B.; Zavattieri, P.D. Additive Manufacturing and Performance of Architectured Cement-Based Materials. *Adv. Mater.* **2018**, *30*, 1802123. [CrossRef] [PubMed]
13. Panda, B.; Ruan, S.; Unluer, C.; Tan, M.J. Improving the 3D Printability of High Volume Fly Ash Mixtures via the Use of Nano Attapulgite Clay. *Compos. Part B-Eng.* **2019**, *165*, 75–83. [CrossRef]
14. Arunothayan, A.R.; Nematollahi, B.; Ranade, R.; Bong, S.H.; Sanjayan, J. Development of 3D-Printable Ultra-High Performance Fiber-Reinforced Concrete for Digital Construction. *Constr. Build. Mater.* **2020**, *257*, 119546. [CrossRef]
15. Khelifi, H.; Perrot, A.; Lecompte, T.; Ausias, G. Design of Clay/Cement Mixtures for Extruded Building Products. *Mater. Struct.* **2013**, *46*, 999–1010. [CrossRef]

16. Marchment, T.; Sanjayan, J. Reinforcement Method for 3D Concrete Printing Using Paste-Coated Bar Penetrations. *Autom. Constr.* **2021**, *127*, 103694. [CrossRef]
17. Salman, N.M.; Ma, G.; Ijaz, N.; Wang, L. Importance and Potential of Cellulosic Materials and Derivatives in Extrusion-Based 3D Concrete Printing (3DCP): Prospects and Challenges. *Constr. Build. Mater.* **2021**, *291*, 123281. [CrossRef]
18. Ducoulombier, N.; Mesnil, R.; Carneau, P.; Demont, L.; Bessaies-Bey, H.; Caron, J.-F.; Roussel, N. The "Slugs-Test" for Extrusion-Based Additive Manufacturing: Protocol, Analysis and Practical Limits. *Cem. Concr. Compos.* **2021**, *121*, 104074. [CrossRef]
19. Li, W.; Ma, H.; Li, Z.; Ma, G.; Guan, J. Cementitious Composites Blending with High Belite Sulfoaluminate and Medium-Heat Portland Cements for Largescale 3D Printing. *Addit. Manuf.* **2021**, *46*, 102189. [CrossRef]
20. Ma, G.; Li, Y.; Wang, L.; Zhang, J.; Li, Z. Real-Time Quantification of Fresh and Hardened Mechanical Property for 3D Printing Material by Intellectualization with Piezoelectric Transducers. *Constr. Build. Mater.* **2020**, *241*, 117982. [CrossRef]
21. Wang, L.; Ma, G.; Liu, T.; Buswell, R.; Li, Z. Interlayer Reinforcement of 3D Printed Concrete by the In-Process Deposition of U-Nails. *Cem. Concr. Res.* **2021**, *148*, 106535. [CrossRef]
22. Sanjayan, J.G.; Nematollahi, B.; Xia, M.; Marchment, T. Effect of Surface Moisture on Inter-Layer Strength of 3D Printed Concrete. *Constr. Build. Mater.* **2018**, *172*, 468–475. [CrossRef]
23. Le, T.T.; Austin, S.A.; Lim, S.; Buswell, R.A.; Law, R.; Gibb, A.G.F.; Thorpe, T. Hardened Properties of High-Performance Printing Concrete. *Cem. Concr. Res.* **2012**, *42*, 558–566. [CrossRef]
24. Perrot, A.; Rangeard, D.; Courteille, E. 3D Printing of Earth-Based Materials: Processing Aspects. *Constr. Build. Mater.* **2018**, *172*, 670–676. [CrossRef]
25. Paul, S.C.; Tay, Y.W.D.; Panda, B.; Tan, M.J. Fresh and Hardened Properties of 3D Printable Cementitious Materials for Building and Construction. *Arch. Civ. Mech. Eng.* **2018**, *18*, 311–319. [CrossRef]
26. Lim, J.H.; Panda, B.; Quang-Cuong, P. Improving Flexural Characteristics of 3D Printed Geopolymer Composites with In-Process Steel Cable Reinforcement. *Constr. Build. Mater.* **2018**, *178*, 32–41. [CrossRef]
27. Panda, B.; Paul, S.C.; Mohamed, N.A.N.; Tay, Y.W.D.; Tan, M.J. Measurement of Tensile Bond Strength of 3D Printed Geopolymer Mortar. *Measurement* **2018**, *113*, 108–116. [CrossRef]
28. Ma, G.; Li, Z.; Wang, L. Printable Properties of Cementitious Material Containing Copper Tailings for Extrusion Based 3D Printing. *Constr. Build. Mater.* **2018**, *162*, 613–627. [CrossRef]
29. Ghourchian, S.; Butler, M.; Krueger, M.; Mechtcherine, V. Modelling the Development of Capillary Pressure in Freshly 3D-Printed Concrete Elements. *Cem. Concr. Res.* **2021**, *145*, 106457. [CrossRef]
30. Liu, C.; Wang, X.; Chen, Y.; Zhang, C.; Ma, L.; Deng, Z.; Chen, C.; Zhang, Y.; Pan, J.; Banthia, N. Influence of Hydroxypropyl Methylcellulose and Silica Fume on Stability, Rheological Properties, and Printability of 3D Printing Foam Concrete. *Cem. Concr. Compos.* **2021**, *122*, 104158. [CrossRef]
31. Zhang, N.; Xia, M.; Sanjayan, J. Short-Duration near-Nozzle Mixing for 3D Concrete Printing. *Cem. Concr. Res.* **2022**, *151*, 106616. [CrossRef]
32. Lu, B.; Li, M.; Wong, T.N.; Qian, S. Effect of Printing Parameters on Material Distribution in Spray-Based 3D Concrete Printing (S-3DCP). *Autom. Constr.* **2021**, *124*, 103570. [CrossRef]
33. Mazhoud, B.; Perrot, A.; Picandet, V.; Rangeard, D.; Courteille, E. Underwater 3D Printing of Cement-Based Mortar. *Constr. Build. Mater.* **2019**, *214*, 458–467. [CrossRef]
34. Lowke, D.; Vandenberg, A.; Pierre, A.; Thomas, A.; Kloft, H.; Hack, N. Injection 3D Concrete Printing in a Carrier Liquid-Underlying Physics and Applications to Lightweight Space Frame Structures. *Cem. Concr. Compos.* **2021**, *124*, 104169. [CrossRef]
35. Jiang, X.; Li, Y.; Yang, Z.; Li, Y.; Xiong, B. Harnessing Path Optimization to Enhance the Strength of Three-Dimensional (3D) Printed Concrete. *Buildings* **2024**, *14*, 455. [CrossRef]
36. *GB/T 2419-2005*; Test Method for Fluidity of Cement Mortar. Chinese National Testing Standard: Beijing, China, 2005.

Disclaimer/Publisher's Note: The statements, opinions and data contained in all publications are solely those of the individual author(s) and contributor(s) and not of MDPI and/or the editor(s). MDPI and/or the editor(s) disclaim responsibility for any injury to people or property resulting from any ideas, methods, instructions or products referred to in the content.